INL/JOU-16-39543
Accepted Manuscript

Reservoir response to thermal and high-pressure well stimulation efforts at Raft River, Idaho

Mitchell Plummer, Jacob Bradford, Joseph Moore, Robert Podgorney

August 2016

Prepared for the U.S. Department of Energy
Office of Nuclear Energy
Under DOE Idaho Operations Office
Contract DE-AC07-05ID14517

Reservoir response to thermal and high-pressure well stimulation efforts at Raft River, Idaho

Corresponding author: Mitchell Plummer[a], Mitchell.Plummer@inl.gov

Jacob Bradford[b], jcbbradford@yahoo.com

Joseph Moore[b], jmoore@egi.utah.edu

Robert Podgorney[a],

[a]Idaho National Laboratory, MS 2107, 2525 Fremont St., Idaho Falls, ID, USA, 83415-2107

[b]Energy & Geoscience Institute at the University of Utah, 423 Wakara Way, Ste. 300, Salt Lake City, UT, USA, 84108

ABSTRACT

An injection stimulation test begun at the Raft River geothermal reservoir in June 2013 produced a wealth of well and reservoir response data. In this paper, we examine the hydraulic response using standard pumping test analysis methods. Analysis of stepped-rate flow tests supports the inference from other data that a large fracture intersects the well in the target reservoir. Pressure – flow response suggests that the flow regime is radial to a distance of approximately ten meters and demonstrates that the pressure build-up cone reaches an effective constant head at that distance. The well's longer-term hydraulic response demonstrated continually increasing injectivity, with the rate of increase varying significantly over time and beginning a long period of rapid increase that started ~2 years after the start of the project and continues to – at the time of this writing - 2.5 years after start of injection. The net change in injectivity is significantly greater than observed in other long-term injectivity monitoring studies, with an approximately 150–fold increase occurring over ~2.5 years. While gradually increasing injectivity is a likely consequence of slow migration of a cooling front, and consequent dilation of fractures, the steady, ongoing, rate of increase is contrary to what would be expected in a radial or linear flow regime, where the cooling front would slow with time. Occasional step-like increases in injectivity, immediately following high-flow rate tests suggest that hydro shearing during high-pressure testing also altered the near-well permeability structure, but such increases have been small relative to the slow steady increases that dominated the injectivity evolution.

Keywords: Well stimulation, injectivity, enhanced geothermal systems[ETB1]

Funding: This work was supported by DOE Grant DE-FG36-08GO18189.

1 INTRODUCTION

Whether to increase productivity of existing hydrothermal reservoirs or to engineer new geothermal reservoirs, methods of stimulating wells to increase productivity are essential to expansion of geothermal energy. To provide a detailed study of well response to stimulation, the Department of Energy (DOE) Geothermal Technology Program (GTP) has sponsored a well stimulation study at the Raft River Geothermal Reservoir in southern, Idaho. An existing well in the Raft River reservoir, well RRG-9, initially drilled to the depth of other productive reservoir wells, proved to have injectivity too low for economical use as either a production well or an injection well. This stimulation project seeks to improve the injectivity of RRG-9 via application of a series of stimulation methods to a sidetracked extension of that well. The stimulation methods include long-term cold-water injection at a variety of flow rates and injection temperatures—aimed at improving permeability by cooling and contraction of the fractured rock host formation—and high-pressure injections designed to alter permeability via application of fluid pressures that exceed the fracture gradient. Methods of monitoring the reservoir include high-resolution temperature logging within the well at all times (via distributed temperature sensing), seismic monitoring, periodic borehole televiewer logging, periodic stepped flow rate tests, and tracer injections before and after stimulation efforts. In this paper, we discuss recent data and analysis from the thermal and high-pressure stimulation efforts, as well as implications for the nature of the fractured reservoir and stimulation efforts in general. Our analysis focuses on use of pumping test data to infer basic hydraulic properties of the reservoir, and how those properties have changed over time.

1.1 Background

The effects of cold-water injection on injectivity have been observed at many sites, but the time scales of such stimulation efforts vary widely. Reinjection of plant effluent in a reservoir with higher initial temperature is, in effect, a long-term stimulation test, with the stimulation temperature defined by plant operating constraints. In several cases, thermal stimulation has been attempted with injection temperatures much colder than the plant effluent temperature, with the stimulation periods on the order of several days to several months. As in this project, stimulation attempts often include thermal stimulation – at varying injection temperatures - and high-pressure stimulation – at a range of injection pressure, and other other stimulation methods may also be attempted. As a result, it can be difficult to distinguish the source of injectivity changes, as well as the mechanisms causing them.

Results of a variety of cold-water stimulation tests demonstrate that the associated changes in injectivity can be significant at both short and long timescales. In a situation similar to that at Raft River, a well drilled for production at the Los Humeros geothermal field was changed to an injector because it was initially unable to sustain productive flow. As a result of three cold-water injection tests in October 2005, the injection flow rate increased by a factor of 26 from its initial value (Flores-Armenta and Tovar-Aguado, 2008). Aqui and Zarrouk (2011) reported on stimulation of a newly completed low-permeability injection well in the Philippines. In that case, while little or no improvement in injectivity was observed following several days of high-pressure injection, subsequent prolonged injection of cooling tower condensates over a period of at least three months, at lower flow rates, resulted in an increase in the injection capacity greater than 100% of the original value. In a review of field data from thermal stimulation tests, Grant et al. (2013) noted that field data commonly demonstrate an injectivity increase that is proportional to t^n, where t is time and n is between 0.4 and 0.7. Clearwater et al. (2015) noted that Grant et al.'s (2013) analytical model of injectivity evolution successfully predicted injectivity changes during startup of the plant at the Ngatamariki geothermal field, New Zealand, which allowed deferral of drilling planned to mitigate an initial injection capacity deficit.

In some cases, cold-water injection periods are alternated with recovery periods or periods of hot-water injection. Tulinius et al. (2000) reported a 50% increase in injectivity following periodic injection of sea water over a period of several weeks in a well at Boulliante, Guadeloupe. Similar discontinuous cold-water stimulation efforts were employed on three production wells at the Sumikawa Geothermal field, Japan (Kitao, 1990). Injectivity improvements obtained were variable, and included some reversals of injectivity gains following return to production flow. At the Salak geothermal field in Indonesia, stimulation efforts applied to wells included alternate injection of cold condensate water and hot brine every 1–4 weeks, with reported increases of approximately 100% in some wells.

Attempts to specifically examine the effect of injection temperature are less common, but Gunnarsson (2011) reported increases in injectivity in the Hellisheidi field, southwest Iceland, of more than six times when the water injection temperature was lowered from 120°C to 20°C—even while viscosity at the injection temperature would have been ~5 times greater. Based on his review of such data, Grant et al. (2013) suggested that a nonlinear relationship exists between injectivity and water injection temperature.

2 MATERIALS AND METHODS

In this study, we examine data from a well stimulation effort at U.S. Geothermal's Raft River site in Cassia County, Idaho, approximately six miles north of the Utah/Idaho border near the town of Malta (Figure 1). This site was heavily studied by the U.S. Department of Energy from 1975 to 1982 and was the testing site of the first commercial-scale binary (isobutene) cycle geothermal power plant in the world. The site is currently producing power from a 13-MW (nominal) binary isopentane power system.

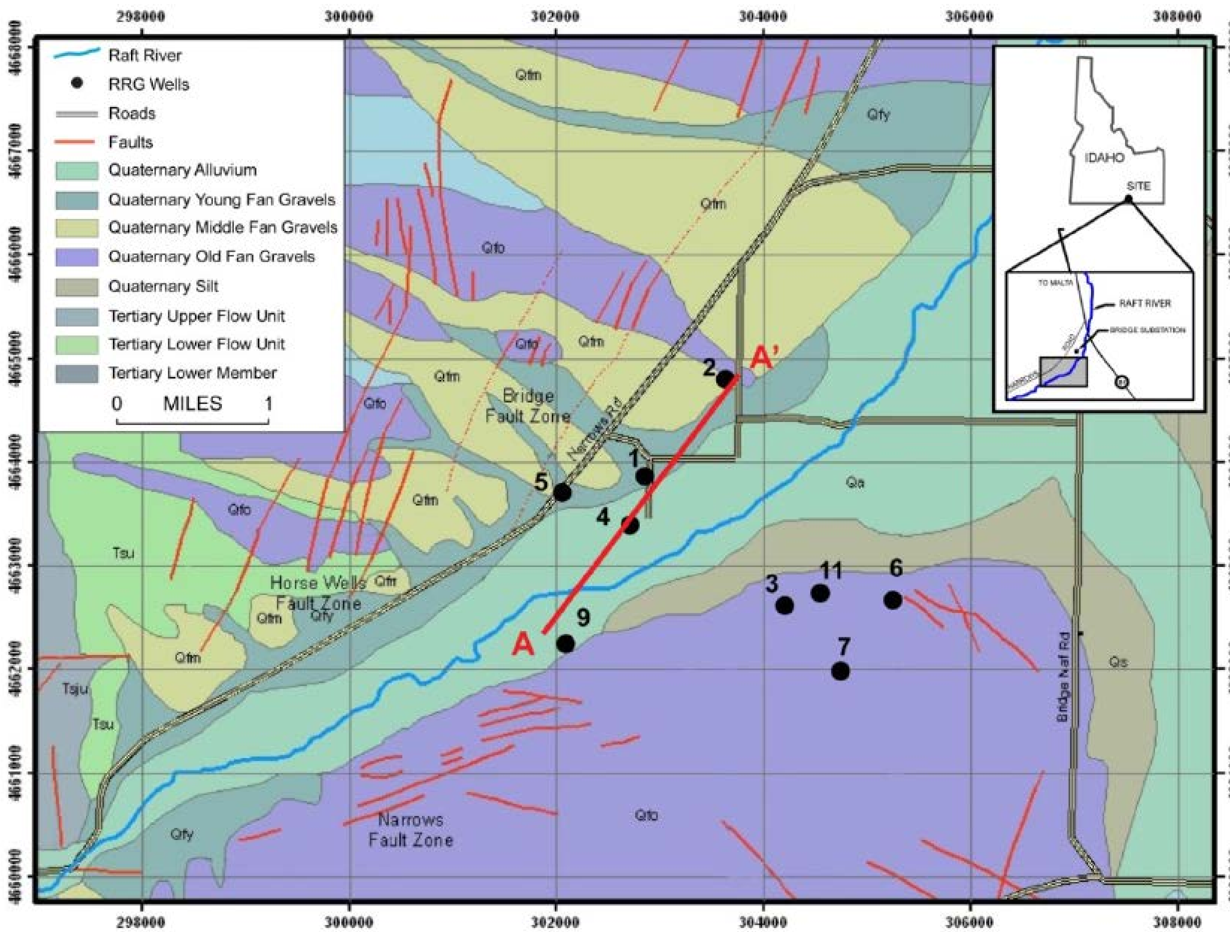

Figure 1. Geologic map of the Raft River geothermal field, with inset map showing general location. Line A – A` shows the location of the cross-section shown as Figure 2.

2.1 Geology

The Raft River geothermal site is located near the southern end of the north-south trending Raft River valley. This valley is characterized by high-angle normal faulting, low-angle faulting emplacing younger over older rocks, moderate plutonism, and the presence of discontinuous metamorphic terrains (Allman et al., 1982). Beneath the surface alluvium, the Salt Lake Formation is a thick (~1200 meter), poorly consolidated deposit consisting of siltstone and sandstone. Underlying this formation is a 150-meter thickness of metasediments, consisting of sub-units of schist and quartzite. The base rock is a Precambrian adamellite. The western side of the valley has been down-dropped along listric faults in the Bridge and Horse Well Fault zones through the Salt Lake Formation. These faults dip 60 to 80 degrees to the east at the surface and become nearly horizontal in the Tertiary sediments. They may have produced many near vertical open fractures at the base of the sediments. Movement along of these faults is believed to have created vertical fractures in the base of the Salt Lake Formation and in the underlying Precambrian metasediments that are responsible for the high well yields in the geothermal field (Allman et al., 1982 and Dolenc et al., 1981).

2.2 Raft River Geothermal Reservoir Operations

Active wells include production wells RRG-1, 2, 4 and 7, and injection wells RRG-3, 6 and 11. Well RRG-5 has generally been operated as an injection well during only the summer months, to provide temporary pressure support to the production wells. Well RRG-9, the focus of this stimulation effort, was inactive prior to this study. The well was initially drilled, in 2007, to a depth of 1856 m (6089 ft), but its productivity was too low for it to serve either as a producer or an injector. As part of this project, a sidetrack, ST-1, was drilled from an exit point at a depth of 1372 m (4500 ft) to a final depth of 1808 m (5932) ft.

121 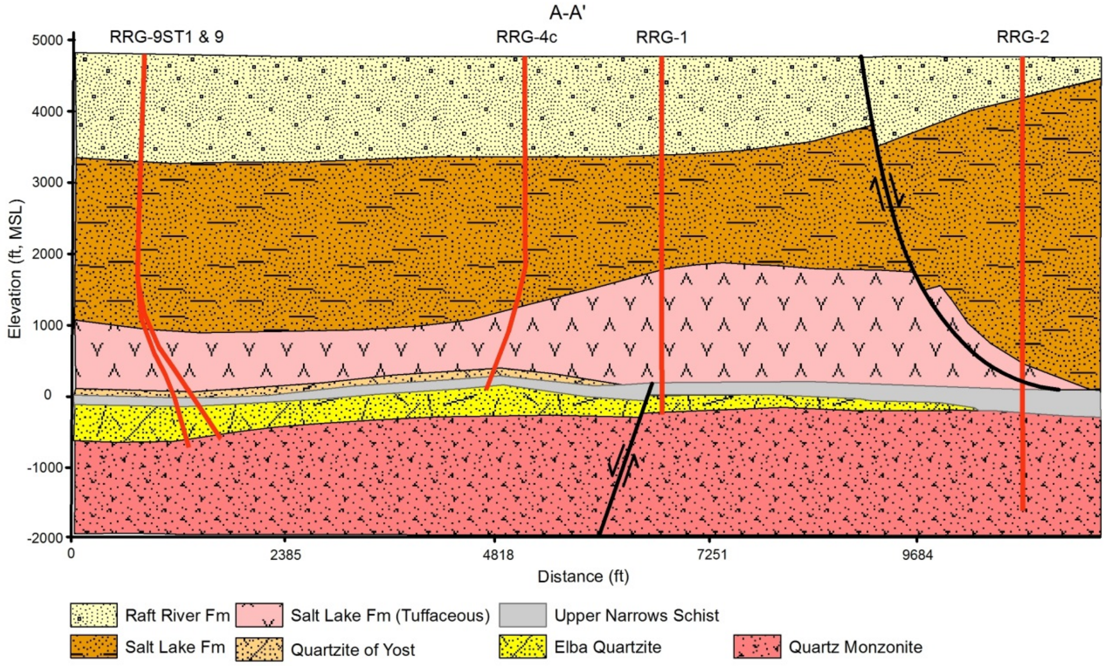

122 Figure 2. Southwest to northeast cross-section of the Raft River geothermal field. Location is shown on Figure 1.

123

2.3 Stimulation at Well RRG-9

A multi-phase stimulation program is in progress at well RRG-9 (Table 1). Phase I of the stimulation began on June 13, 2013, with injection from the power plant at a temperature of about 39°C, pressure of 275 psig, and flow rate of approximately 40 gpm. That injection continued until August 20, 2013, and was immediately followed by a stepped-rate injection test on August 22, 2013, prior to initiation of the next phase of injection. The stepped-rate test was aimed at detecting differences in reservoir behavior as compared to a similar test conducted on February 24, 2012, well before Phase I of the stimulation. In Phase II, two positive displacement plunger type pumps were used to increase the injection pressure and flow rate for about one month. The highest rate achieved was 261 gpm at a pressure of 809 psig. During this time, fluid from the cooler water well was injected in a series of steps at an increasing flow rate. The pumps were then removed and plant injection resumed on September 25, 2013, and continued until March 30, 2014. Flow rates and wellhead pressures during the latter period were approximately 122–133 gpm at 272–281 psi. Between April 1 and April 3, 2014, high-pressure

Table 1. Injection history during the stimulation phases at well RRG-9.

Fluid Source	Booster Pump(s)	Time Period	Flow Rate (gpm)	Average WHP (psi)	Average Fluid Temperature (°C)
Mixed	Yes	2-24-12	Stepped rates		
Plant injectate	No	6-13-13 to 8-20-13	43	280	39
Mixed	Yes	8-22-13	Stepped rates		
Plant injectate	No	8-23-13 to 8-30-13	141	540	40
Plant injectate	Yes	9-1-13 to 9-8-13	261	809	46
Cold Well Water	Yes	9-12-13 to 9-16-13	254	743	12
Cold Well Water	Yes	9-16-13 to 9-24-13	191	522	13
Plant injectate	No	9-25-13 to 12-2-13	122	272	30
Plant injectate	No	12-3-13 to 3-30-14	133	281	27
Mixed	Yes	4-1-14, 4-3-14	Stepped rates		
Plant injectate	No	4-4-14 to present (10-1-15)	133	281	27

injection testing via a series of steps at a constant injection rate was conducted, to attempt to increase permeability via hydroshearing of existing fractures in the vicinity of the well.

2.4 Stimulation Monitoring Methods

Flow rates to the well are measured at the plant and at the well head. Injection rate, wellhead pressure, and surface temperature have been monitored on a nearly continuous basis since June of 2013. Pressure transducers are located on both the 10-inch injection pipeline, near the RR-9 ST1 wellhead, and on the wellhead itself, and both of these devices also monitor temperature. A distributed temperature sensing cable (DTS) placed in the well has been used intermittently since June 2013. A pressure sensor, located at the bottom of the DTC cable was incorporated to monitor downhole pressure, but that device failed during installation. In April 9, 2015, the DTS cable was removed and a pressure sensor was placed just above the casing shoe (5,551 ft. MD) to monitor near bottom-hole pressures. Initially, flow rates were monitored by an orifice plate meter. However, initial flow through the 10-inch line, June 13, 2013 to July 23, 2013 was not high enough to be measurable by that device. An ultrasonic flow meter was installed, July 23, 2013, on the 3-inch line to correct this deficiency. On November 14, 2013 the ultrasonic flow meter stopped working properly and was replaced, on February 7, 2014, by an orifice plate meter on the 10-inch line. By then, flow rates through the 10-inch line were sufficient to obtain accurate readings from this device. An 8-station microseismic array was placed around RRG-9 ST1 in May 2013. Each station consists of a geophone cemented in a 300 ft. borehole. In response to microseismic activity to the northeast some microseismic stations were repositioned in 2016.

3 RESULTS AND DISCUSSION

While the stimulation project includes seismic monitoring, high-resolution temperature monitoring, and other monitoring efforts, this study focuses on the implications of the most direct measure of the hydraulic response of the reservoir—the relationship between pressure and flow. High-resolution monitoring of pressure is not available in operational production and injection wells, so pressure data is essentially available only at RRG-9. We therefore employ single-well pumping test analyses to interpret the hydraulic response data. The relatively simple geometric models for flow (e.g., linear, radial, and spherical flow models) of analytical solutions, however, provide a useful reference for estimating how more complicated geometries might apply.

3.1 Injectivity Measures

The most notable features in the pressure response to stimulation injections are the gradual increases in injectivity (evident as increases in flow rate at constant pressure) that occur during most of the ~2.3 years of injection. These changes are best illustrated by examining an injectivity index plot (Figure 3), in which the injectivity index is a lumped parameter that incorporates both well performance and reservoir permeability. For a steady state radial flow problem, described by the Thiem equation (Thiem, 1906 and Kruseman and deRidder, 1994), for example, the well injectivity would be

$$Injectivity = \frac{Q}{\Delta P} = \frac{2\pi K b}{\ln(\frac{r_{well}}{r_{constant}})\,\mu} \qquad \text{(Eq. 1)}$$

The injectivity index thus assumes that pressure changes associated with flow at the well have propagated to the point at which the rate of change due to pressure diffusion is negligible, and further changes in wellhead pressure are due to changes in well efficiency, fluid viscosity, and reservoir permeability.

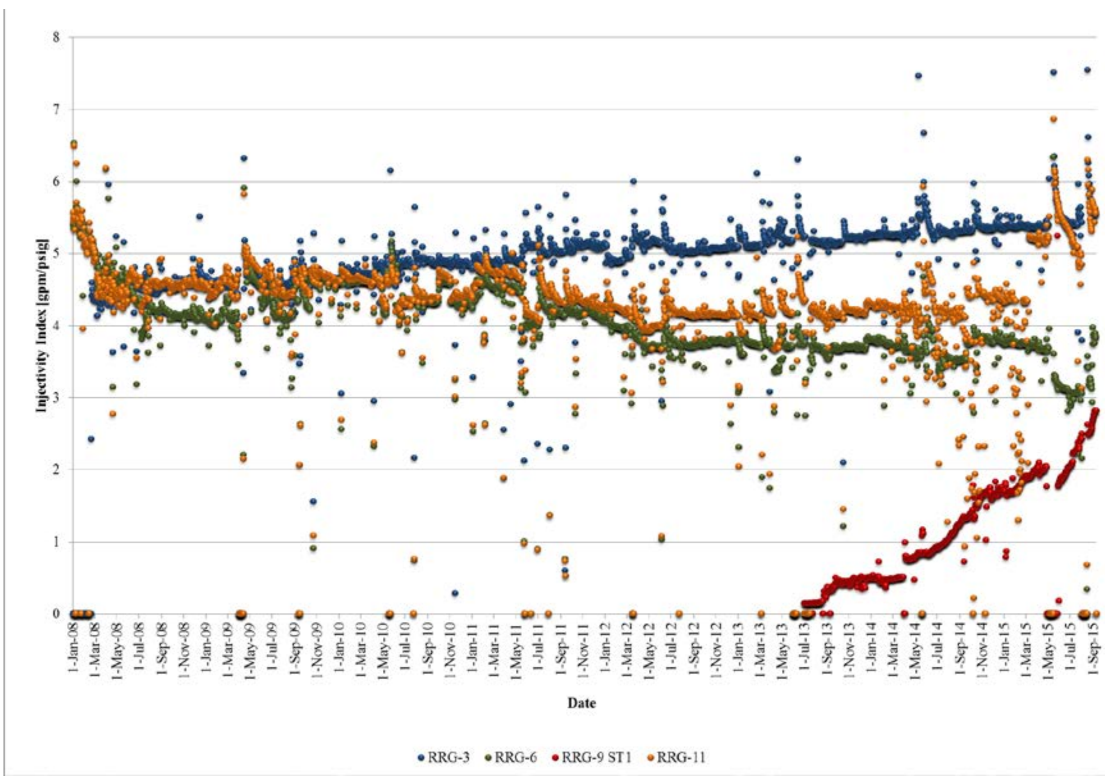

Figure 3. Injectivity index for RRG-9 and the three primary injection wells in operation since startup in 2008.

Another common measure of well performance over time, a modified Hall plot (Earlougher, 1977), is provided as Figure 4. The Hall plot, in which cumulative flow is plotted against cumulative bottom-hole pressure, is a time-integrated, and thus, smoothed, measure of injectivity (Equation 2). In the equation, p_{tf} is the wellhead pressure, t is time, p_e is the reservoir pressure, Δp_w is the hydrostatic pressure, μ is the viscosity, p_D is the dimensionless pressure, s is the skin factor, k is the permeability, h is the formation height, and W_i is the cumulative volume injected. In the Hall plot, concave curvature denotes decreasing injectivity and convex curvature shows increasing injectivity. From Equation 2, the slope of the line (m_H), given in Equation 3, is proportional to the skin effects of the wellbore and inversely proportional to the permeability (Earlougher, 1977).

$$\int_0^t p_{tf}\,dt - (p_e - \Delta p_w)t = \frac{141.2\mu(p_D+s)}{kh} W_i \quad \text{(Eq. 2)}$$

$$m_H = \frac{141\mu(P_D+s)}{kh} \quad \text{(Eq. 3)}$$

From Equation 3, convex or concave behavior of the plotted line can be directly related to changes in reservoir properties. For example, convex behavior is indicative of a decreasing skin factor around the well and/or increasing permeability. The Hall plot allows for relatively complex trends in injectivity to be readily identified while providing insight into the changing reservoir properties behind those changes.

Note that both of these measures of injectivity mathematically assume a constant radius of influence, whereas—for an infinite acting cylindrical reservoir—the radius of influence grows in proportion to the square root of time; injectivity, therefore, decreases with time. The error in assuming a constant pressure at some arbitrary distance would thus lead only to slight underestimation of the actual injectivity change.

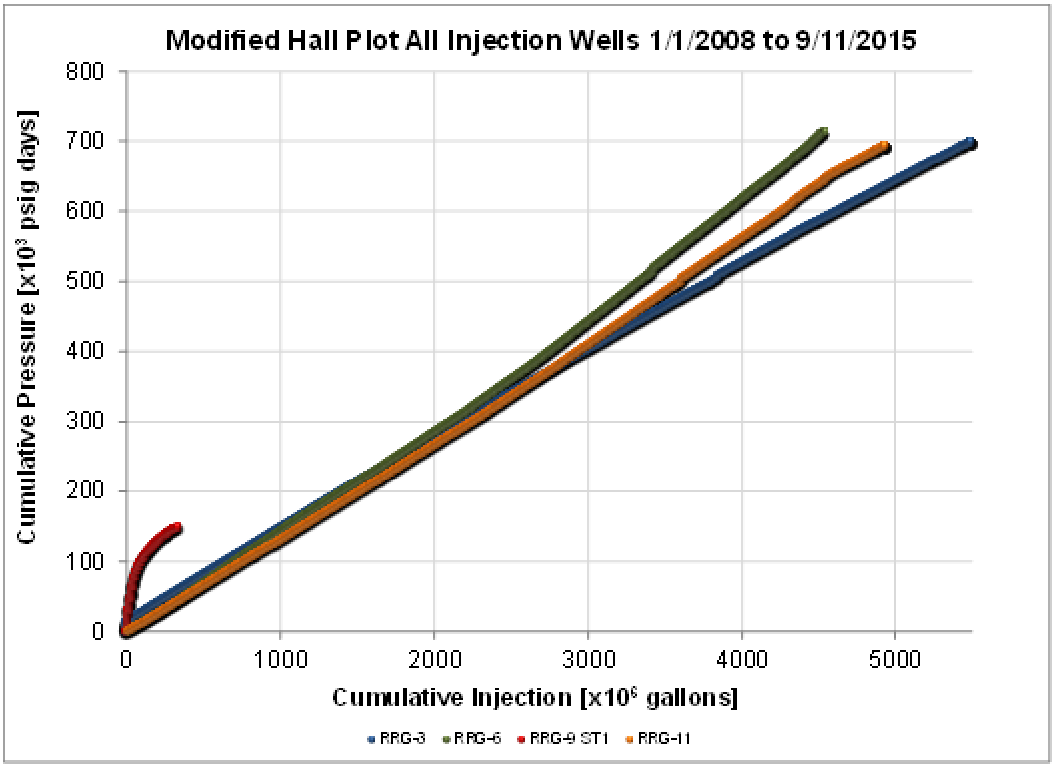

Figure 4. Modified Hall plot for RRG-9 and other primary injection wells at Raft River. Convex curvature in these plots indicates increasing injectivity. The convex curvature shows an increase in permeability and/or a decrease in the skin factor around the well.

3.2 Injectivity Evolution

Injectivity increased at a steady but relatively slow rate until June, 2014, following a temporary shutdown. At that time, injectivity began to increase significantly. During the second hydraulic stimulation, the injectivity index increased by 33 $cm^3\ s^{-1}\ MPa^{-1}$ (3.6E-3 gpm psi^{-1}) per day. Following the second stimulation, injection from the plant was resumed until the third hydraulic stimulation in April of 2014. Over this time period, the injectivity index grew by only 0.21 $cm^3\ s^{-1}\ MPa^{-1}$ (2.3E-5 gpm psi^{-1}) per day. After the third hydraulic stimulation, the injectivity index began to increase much more rapidly, at a rate of 180 $cm^3\ s^{-1}\ MPa^{-1}$ (2.0E-2 gpm psi^{-1}) per day. A falloff test conducted in April and May of 2015 was followed by another step increase in the injectivity index. At the time of this study, 2.25 years after the start of injection, the injectivity index continues to increase, at a rate of 91 $cm^3\ s^{-1}\ MPa^{-1}$ (1.1E-2 gpm psi^{-1}) per day.

The overall trend, over more than two year of injection, has been a growing rate of increase in injectivity with time. Based on a review of field data, Grant et al. (2013) noted that cold-water injection in geothermal fields has generally produced an increase in injectivity that is proportional to t^n, where n is between 0.4 and 0.7. Here, we observe several periods of markedly different duration and rate of increase, with an overall increase that has not, to our knowledge, been observed in other studies of injection well performance. Histories of other injection wells in the Raft River geothermal field, though not seated in the same reservoir, did not exhibit similar changes in injectivity following startup (Figure 4).

Because the timescale of the larger increases in injectivity is similar to that expected for cooling front migration, we infer that those changes are a result of the slow migration of the cooling front away from the well and the consequent contraction of rock and expansion of fractures. The apparent acceleration of the rate of increase is, however, contrary to what might be expected in a homogeneous system. Depending on its mechanical response to cooling, the effect of cold-water injection on the formation may include dilation, shearing, or extension of existing fractures. Consequent improvement in injectivity may result from one of two mechanisms. The first of these involves improving or creating permeability along pathways that intersect more productive, higher-permeability regions of the system. The probability of producing such distal effects can be expected to increase as the cooling front migrates outward from the well, as the number of intersected fractures increases. The second is near-well enhancement of permeability that consequently reduces pressure gradients near the well, where pressure gradients are greatest. Thus, proximal cooling can improve well productivity, even if no distal connections to regions of higher permeability are made.

Because the probability of producing connections to zones of greater permeability increases as the cooled region expands, it is helpful to have some estimate of the likely migration rate of the cooling front in order to understand the length scale that might be involved in determining how its position might impact permeability and, thereby, pressure change at the well. Flow from RRG-9 is likely conducted by a relatively complicated fracture pattern. When the injection flow is divided among many fractures, propagation of the thermal front is inversely proportional to the number of fractures and is retarded relative to the fluid injection front by a factor that depends on porosity. That is, the greater the heat exchange with the rock, the slower the cooling front migration. For a porous medium, the thermal front is steep, and its retardation factor is

$$1 + \frac{C_{p\_r}(1-\theta)}{\theta C_{p\_f}} \quad \text{(Eq. 4)}$$

(Palmer et al., 1992) where C_{p_r} and C_{p_f} are volumetric heat capacities for the solid and fluid, respectively, and θ is porosity. For a uniformly fractured system, the thermal front is more diffuse for lower fracture density, but the average retardation factor is similar to that for the porous medium. Using the average fracture density of the section of Elba Quartzite seen in the borehole televiewer data (~0.9 fractures per meter), and assuming a fracture aperture of 0. 01 to 0.1 mm, the thermal front would lag the fluid front by a factor of approximately 8E3 to 8E4. Thus, the cooling front in a 1D flow system as described above, with the same flow conducted equally by ~160 fractures, would migrate through a particular fracture network only after 8E3 to 8E4 pore volumes of fluid had passed through the same network. Using similar calculations to estimate cooling front propagation, and including the effect on fracture dilation, Plummer (2013) showed that injectivity would, as described by Grant (2013), generally be expected to increase at a lesser rate with time, for both radial-flow systems and linear-flow systems. Those calculations, however, presume an infinite reservoir. Here, we hypothesize that the expansion of the cooling front creates an increasingly larger area of connection with a region of constant pressure, either the drawdown cone of the production wells or a region of considerably greater permeability independent of the production zone. Further investigations will consider whether such interactions could produce, over a period of several years, an accelerating rate of injectivity increase with time.

Distinct jumps in injectivity also occurred following the two high-pressure injection tests in August 2013 and April 2014. We interpret those rapid changes as near-well permeability increases associated with hydro shearing of fractures or mitigation of well skin effects developed during drilling. Following a pressure falloff test in the spring of 2015, the rate of injectivity increase has increased substantially from the previous rate of growth. It is hypothesized that this increase in injectivity is due to self-propping of the intersecting fracture zone.

3.3 Pressure Transient Analysis

The reservoir's response to the stimulation efforts is evident in several features of the long-term flow and pressure record, which each provide information about a different timescale or different aspect of behavior. At the shortest timescale, pressure response curves during the stepped-rate pressure tests have a shape that suggests a radial flow regime. The pressure response (Figure 5) to the first step of the first stepped-rate test (February 2012), which should be representative of initial conditions in the reservoir, demonstrates a shape that is typical of radial flow in an infinite aquifer. We used the commercial package Aqtesolv (Duffield, 2007) to test a variety of reservoir response models, including, for example, models incorporating vertical and horizontal fractures, aquifers with leakage from surrounding formations, partial penetrating wells, and wellbore storage. Results demonstrated that the Theis-Hantush (1961a,b) type curve, or similar models assuming essentially uniform radial flow, provided substantially better fit than spherical flow models, linear flow models, or models including some simple heterogeneity. This is largely consistent with general understanding of the stratigraphy, which indicates that the main production zone is the Elba quartzite, a roughly horizontal unit with a thickness of approximately 200 meters. While partial penetration effects were included in the solution, because the well is cased through the upper 42% of that unit, the effect of that on the calculated hydraulic parameters is insignificant, except that it allows some estimation of vertical to horizontal anisotropy. Models incorporating a small well storage factor provided slightly better fit, but as there was no mechanism to provide the magnitude of the inferred storage, we conclude that the better fit is primarily a result of additional degrees of freedom, not storage. Fitting the Theis-Hantush (1961a,b) partial penetration model to the data suggests a transmissivity (permeability times thickness) of 3.1E-14 m^3 (1.5E-6 m^2 s^{-1}) and a storativity of 4.3E-6 m Pa^{-1} (0.042 m m^{-1}). The implied rock permeability and compressibility depends on the thickness of the fractured rock available for flow. Based on an estimated thickness of approximately 200 m for the Elba Quartzite, the implied transmissivity and rock compressibility are 1.7E-12 m^2 (8.2E-9 m/s) and 2.4E-8 Pa^{-1} (2.3E-4 m^{-1}), respectively. The latter value is on the high end of expected values of compressibility. Domenico and Schwartz (1990), for example, indicate that coefficients of vertical compressibility of jointed rock range from 6.9E-10 Pa^{-1} to 3.3E-10 Pa^{-1}, while Freeze and Cherry (1979) report a much wider range of values, from 1E-10 Pa^{-1} to 1E-08 Pa^{-1}.

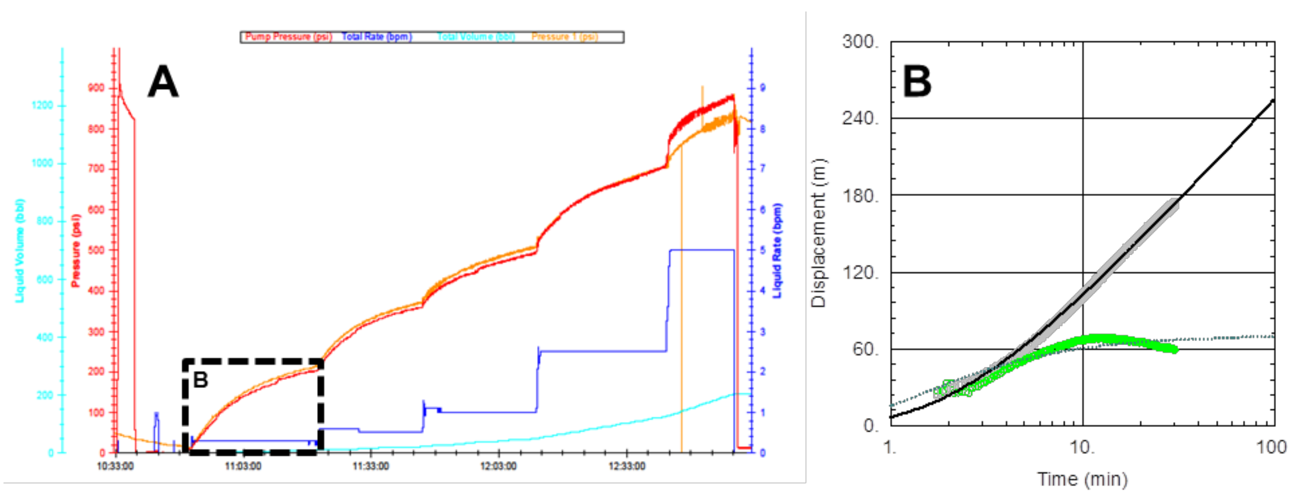

Figure 5. (A) February 24, 2012 step rate test conditions from 10:33 to 13:00. Dark blue and light blue lines represent the liquid pumping rate and cumulative volume, respectively. Red and orange lines are measured pressures. (B) Best-fit Theis-Hantush, partial penetration, solution (curves) from first step of test (symbols), plotted in semi-log space to illustrate radial flow behavior. Gray symbols & black curves are hydraulic head displacement; green lines and symbols display derivative, $\left(\frac{ds}{d(\log t)}\right)$.

The magnitude of the rock compressibility is important for inferring the effect of injection on other wells in the reservoir, on possible surface deformation that might be measured via GPS or InSAR, because it controls subsurface expansion due to pressurization. Unfortunately, single well pumping tests only offer an uncertain estimate of compressibility because it is exclusively inferred from the rate of pressure response, and is thus convoluted by other factors that affect that rate. Because one of these factors is effective well radius, the anomalously high storativity calculated from the pressure response may actually be an indication of the spatial extent of a large fracture that is known to intersect well RRG-9 in the Elba Quartzite. High spatial resolution temperature monitoring of the well during cold-water injection suggests that most of the injected water enters the formation over an interval between 1719 m (5640 ft) and 1725 m (5660 ft), and a large fracture appears in the televiewer logs at that depth. If a fracture with anomalously large aperture intersects the borehole, it increases the effective well radius because it increases the maximum radial position near the well at which pressure gradients are effectively negligible compared to that in larger formation. A large fracture can readily have that effect because transmissivity increases as the cube of fracture aperture, so only a small increase in aperture is needed to significantly reduce the local pressure gradient. Information about the extent of such a fracture at RRG-9 might be inferred, because *u* in the Theis equation for drawdown, $s = \frac{Q}{4\pi T} W(u)$, is a function of well radius as well as storativity, transmissivity, and time: $u = \frac{r^2 S}{4Tt}$. For that reason, effective well radius is sometimes included as a term in the well function argument, *u*, though generally as a reduction in radius due to well screen skin effects.

The effective radius is related to the actual radius by

$$r_w{}^2 S = r_e{}^2 S_{actual} \text{ (Eq. 5)}$$

where r_w is the actual well radius, *S* is the curve-fit specific storage, r_e *is* the effective well radius, and S_{actual} is the actual rock compressibility. Thus, storativity values that are anomalously high by one to two orders of magnitude may simply reflect three- to ten-fold increases in effective well radius. If we, therefore, assume that the rock compressibility around RRG-9 is in the typical range of 2E-10 Pa^{-1} to

2E-9 Pa^{-1}, we could infer that the large fracture intersecting the well is anomalously large to a radial extent of 0.4 to 1.1 meters. This is useful information, as some previous studies generating hypothetical fracture distributions based on fractures identified in RRG-9 have assumed that fracture to be continuous to a radius of hundreds of meters.

3.3.1 Analysis of First Step of Each Stepped-Rate Test

A period of radial-flow behavior is evident in each of the four stepped-rate pumping tests conducted. In many tests, however, the same hydraulic parameters do not provide a fit to the superposition of the response through subsequent steps, and the differences are greater than are typically accounted for using variable well efficiency. Superposition calculations using step-varying hydraulic parameters provide a reasonable fit to the observations and are consistent with a slight hydraulic jacking effect, in which fractures that intersect the well expand with increasing pressure to increase the effective well radius. We, therefore, calculated initial hydraulic parameters for each test from the response to the first step, for which other factors should be negligible. In the 8-22-14 test, non-steady pumping during the first hour made it difficult to interpret that response period, and we used, instead, the response to the second step. To allow a proper fitting range for storativity in these analyses, we assumed an effective well radius of 10x the actual radius, which effectively reduced the magnitude of the calculated storativity by 100x.

Consistent with the injectivity plot, results (Table 2) indicate that transmissivity at the well increased significantly during the project, although the pumping tests data show a different magnitude of change. Transmissivity appeared to have improved 7-fold between the first, pre-stimulation, test and the August 2013 test, while the injectivity increased by a factor of only 1.7 over that period. Then, while the April 2014 tests yielded transmissivity estimates 16 to 95 times greater than during the pre-stimulation test, the injectivity values prior to, and immediately following, the April test were only 3.3 and 5 times greater than the initial injectivity. Because the pumping test analysis focuses on the early time pressure-transient data, we attribute the difference in apparent response to differences in the radius of influence for the different measures. The pumping test analyses are more strongly affected by changes proximal to the well, while the injectivity changes measure more distal effects. That the proximal effects would be greater is consistent with the fact that the highest injection pressures exist nearest the well and that thermal contraction effects on fracture aperture would be greatest in the zone where cooling is most extensive.

As Rutqvist (1998) demonstrated, pumping rate tests conducted at different pressures allow calculation of the vertical compressibility of the rock from the change in transmissivity-based aperture estimates:

$$S = \frac{\rho_f g}{f} \frac{\partial b_h}{\partial p}$$, (Eq. 6)

where b_h is hydraulic aperture and f is a correction factor that compensates for the difference between a natural, rough fracture, and the ideal fracture of smooth parallel walls. The best data for such a calculation comes from the combination of data from the initial steps of the stepped-rate tests conducted on 4-1-14 and 4-3-14, because the flow rates differed by a factor of two and the hydraulic parameters estimates for each are not influenced by the pressure buildup associated with earlier steps. Based on those data, and assuming a correction factor, f, of 0.3, the compressibility of the reservoir is approximately 8E-9 Pa^{-1}, which is consistent with our assumption that the storativity calculated from the first step of the first test reflects some increased effective well radius.

Table 2. Pressure-transient test conditions and hydraulic parameters estimated from pumping tests conducted during the stimulation of well RRG-9. Calculations assume an effective well radius of 1.1 m and partial well penetration of 76 m in a 200-m thick aquifer.

Injection Test Date	Pumping Period (min)	Flow Rate (m^3 s^{-1})	Flow Rate (gpm)	Transmissivity (m^3)	Storativity (m Pa^{-1})	Permeability (m^2)	Compressibility (Pa^{-1})	Final Excess Pressure (MPa)
2/24/12	0 - 30	8.3E-04	13.2	3.1E-14	4.7E-08	1.5E-16	2E-10	1.7
8/22/13	70 - 197	5.9E-03	93.3	4.9E-11	2.8E-06	2.5E-13	1E-08	4.2
4/1/14	0 - 68	1.3E-02	210	5.2E-13	4.3E-06	2.6E-15	2E-08	1.1
4/3/14	0 - 51	2.6E-02	420	4.5E-13	3.1E-06	2.3E-15	2E-08	1.9
4/1/14	0 - 200	5.3E-02	840	6.8E-13	3.1E-06	3.4E-15	2E-08	5.8
4/3/14	0 - 200	7.9E-02	1260	7.4E-13	2.1E-06	3.7E-15	1E-08	6.8

The distance over which fluid pressure increases are felt depends largely on hydraulic diffusivity of the fractured rock, which depends, in turn, on the thickness of the fractured rock reservoir, its compressibility, and its permeability. A Theis-curve-like response over a period of 1 hour, as evident in the pumping test data, indicates relative uniformity over a radial distance that depends on the hydraulic diffusivity, the ratio of transmissivity to storage capacity. Data from longer constant rate periods indicates that apparent radial flow behavior persists for approximately 200 minutes. At that short timescale, for a compressibility of 2E-10 Pa-1 to 2E-8 Pa-1 and the inferred transmissivity of 3.1E-14 m^3 (8E-7 $m^2\ s^{-1}$ < hydraulic diffusivity < 8E-5 $m^2\ s^{-1}$) , the radial distance at which 1% of the injection displacement pressure would be reached would be between 2 and 17 meters.

According to the radial flow model implied by the above analysis, pressure would continue to increase during constant injection, but at a rate that diminishes with time. This is contrary, however, to what is observed in longer-term pressure response, even neglecting the long-term increases in well injectivity that occurred. Figure 6 illustrates well response during a 12-day period in early September, 2013 in which the flow rate changed dramatically on several occasions, and which evidences long-term pressure response to initially steady flow. At 3.5 days into this record, the well returns to steady injection after a period of greatly reduced injection rate; after 8 days, the well recovers to zero gage pressure after a long period of steady flow and pressure. In each case, the pressure appears to reach steady state in approximately 18 hours.

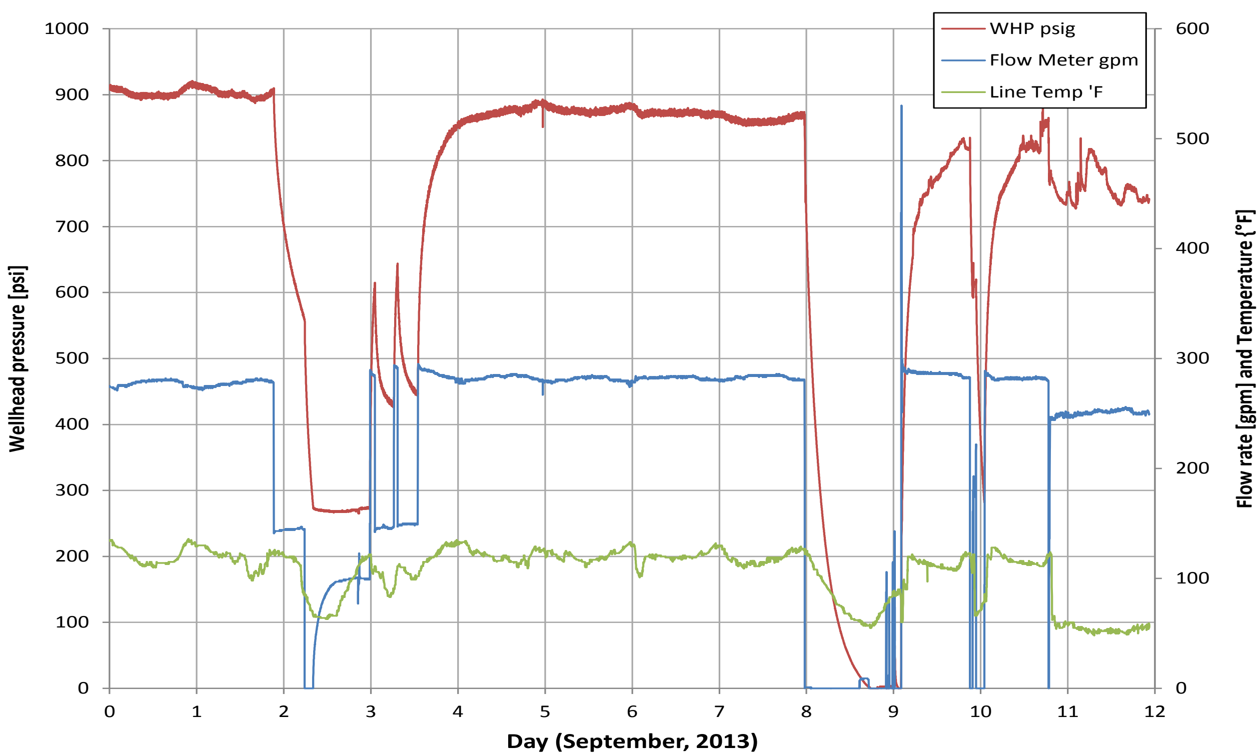

Figure 6. Wellhead pressure, injection rate, and injection line temperature during a 12-day period in early September, 2013, evidencing long-term pressure response during two ~1-day periods following a large change in flow rate.

The longest constant-flow period available for analysis during that period is the pressure response to resumption of a constant rate injection at 287 gpm from a hydrostatic condition, shown in Figure 7. Again, the early time data suggests a radial flow regime, as demonstrated by the excellent fit to a Theis solution in observations up to 200 minutes of injection. At that time, there is a strong departure from that curve, and the rate of pressure increase after that point is much slower than would occur in a uniform radial flow scenario. This suggests heterogeneity in the reservoir that provides either greater diffusivity at a relatively short distance from the well or interception of a region of increased pressure. This could be due to a change to a more spherical flow regime or interception of a more permeable zone in one or more directions from the well. A derivative plot (Figure 7), which is commonly used to infer boundary condition effects, shows that $\frac{ds}{d(\log t)}$ transitions, at ~200 minutes, from a constant value to a decreasing value with slope of approximately -1, which can be interpreted as evidence that the pressure field has effectively encountered a constant head boundary (Fekete, 2009).

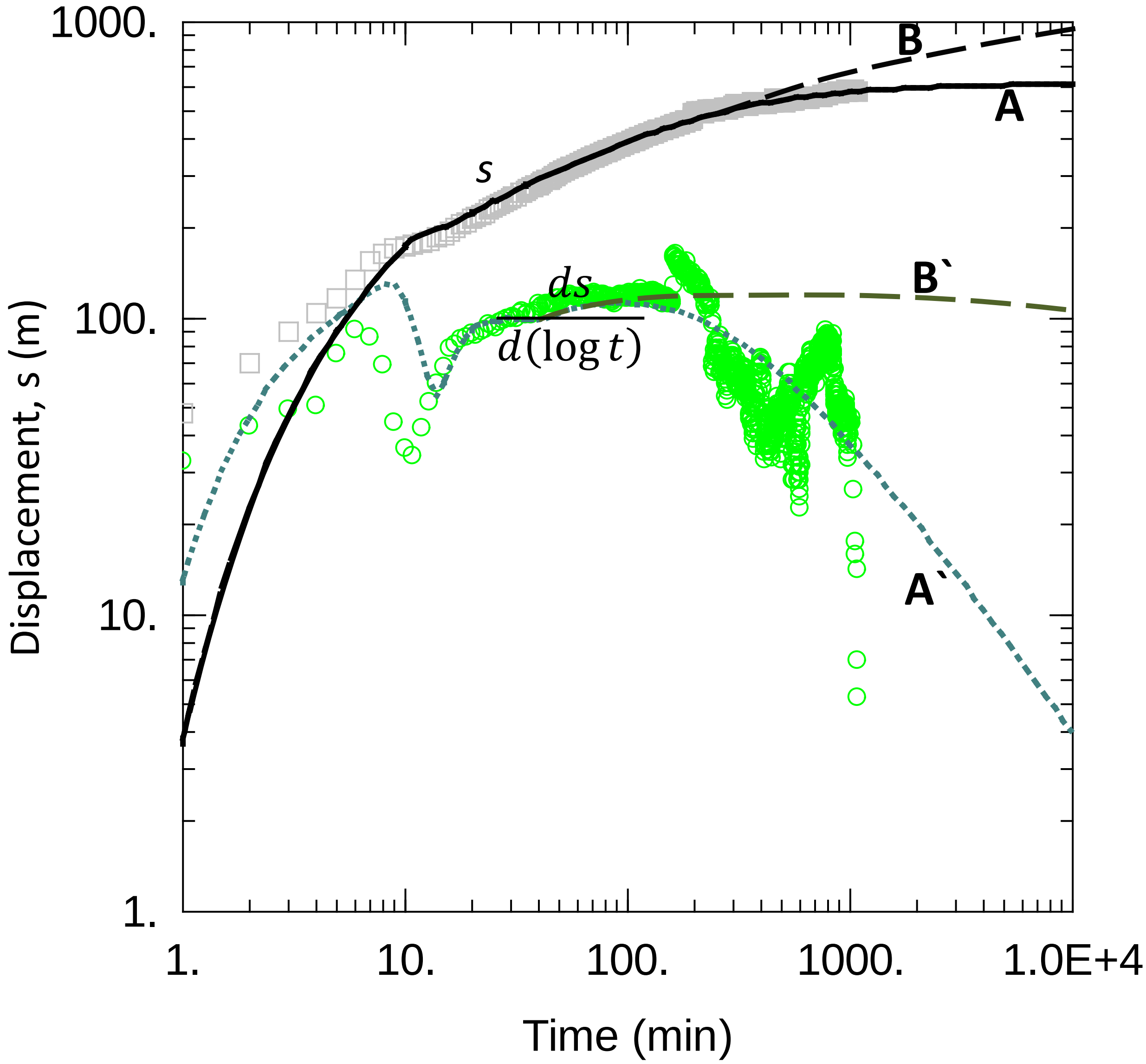

Figure 7. Displacement, s, and ds/d(log(t)) for restart of injection on September 9, 2013, for constant injection rate of ~287 gpm. Symbols show observations for (squares) displacement and (circles) ds/d(log(t)). Curves represent best-fit parameters for s and ds/d(log(t)) for a Theis solution with (A & A`) a constant head boundary located 7 m from the well and for (B & B`) the standard infinite aquifer solution.

Estimates of the hydraulic diffusivity of the reservoir provide some constraint on the distance to a hypothetical constant-heaad boundary. Based on those estimates, the effective radius of influence of the injection (i.e., the radial distance at which pressure has returned to ambient reservoir pressure), after 200 minutes, would be approximately three meters. To illustrate how a model with heterogeneity can better reproduce the observed pressure response, we show results of an analytical (1D radial flow) solution that incorporates a constant pressure boundary and provides a reasonable fit to the data. To estimate the distance to the hypothesized region of greater transmissivity, we introduce a boundary into the radial flow solution and vary the distance to it as a fitting parameter. In this model, we assume a relatively low hydraulic diffusivity in the near-well region in order to reproduce the slow rise of pressure at an early time. That low diffusivity, which results in a slow rate of pressure increase away from the well implies, in turn, that the more transmissive region that causes the inflection at 200 minutes is relatively near the well. In this case, placing a constant head boundary at a distance of seven meters creates a pressure response curve that reproduces the observed response. In a 2D flow model, inclusion of simple heterogeneity would produce a similar response.

Additional information about reservoir hydraulic properties comes from a plant shutdown period that allowed collection of well interference data involving well RRG-9. Pressure-transient evidence indicates that RRG-9 responded to a temporary shutdown of the production and injection wells in May 2015 (Figure 8). Six days prior to a plant shutdown on May 4, 2015, well RRG-9 was shut in so that pressure changes associated with plant shutdown might better be detected at that location. Following shut-in of RRG-9, its pressure fell at steadily declining rate, but began to rebound approximately 4 days after shutdown of the plant and its production and injection wells. The plant wells (excluding RRG-9) were restarted 12 days after shutdown, and although pressure in RRG-9 continued to rise, the rate of increase began to decline approximately 4 days after that restart. Pressure at RRG-9 thus appears to be affected by pressure at the production wells, >=1.2 km distant. This is consistent with the fact that the primary hydraulic formation in RRG-9 is believed to be the same unit that supplies the primary production wells. The lag in the response of RRG-9 to the shutoff of the production wells is consistent with the time required for a larger, locally induced pressure change to decay to the magnitude of the slowly increasing effect of a more distant pressure change. To illustrate that behavior, we compare, in Figure 8, the observed response to simulated pressure response in a relatively simple 2-well model with a single homogeneous aquifer sandwiched between aquicludes, with pumping history, interwell distances, and well construction similar to that employed at Raft River. A reasonable fit to the much of the observed response is obtained by adjusting only hydraulic diffusivity (0.5 $m^2\ s^{-1}$) and a well skin factor (100) at RRG-9, with the latter value effectively providing some of the heterogeneity needed fit both the initial pressure decline after shutoff of RRG-9 and the response at that location to stopped extraction 1.3 km away.

This apparent response of RRG-9 to production well perturbations is important because it demonstrates a hydraulic connection between RRG-9 and the production reservoir and demonstrates the potential for

RRG-9 to provide pressure support for production. This is consistent with tracer recovery data, which indicates that the first arrival of tracer injected at RRG-9 didn't reach the closest production well (RRG-4) until 490 days later. As the shortest path between those two wells is ~1.3 km, this indicates an average seepage velocity of approximately 2.4 m day^{-1}. As an indication of the type of system that would yield such a long travel time, we note that a single continuous fracture of 0.1 mm aperture, with a total pressure drop of 70 psi over 1.2 km would yield that seepage velocity. For comparison, the pressure difference between RRG-9 and the production wells is on the order of several hundred psi.

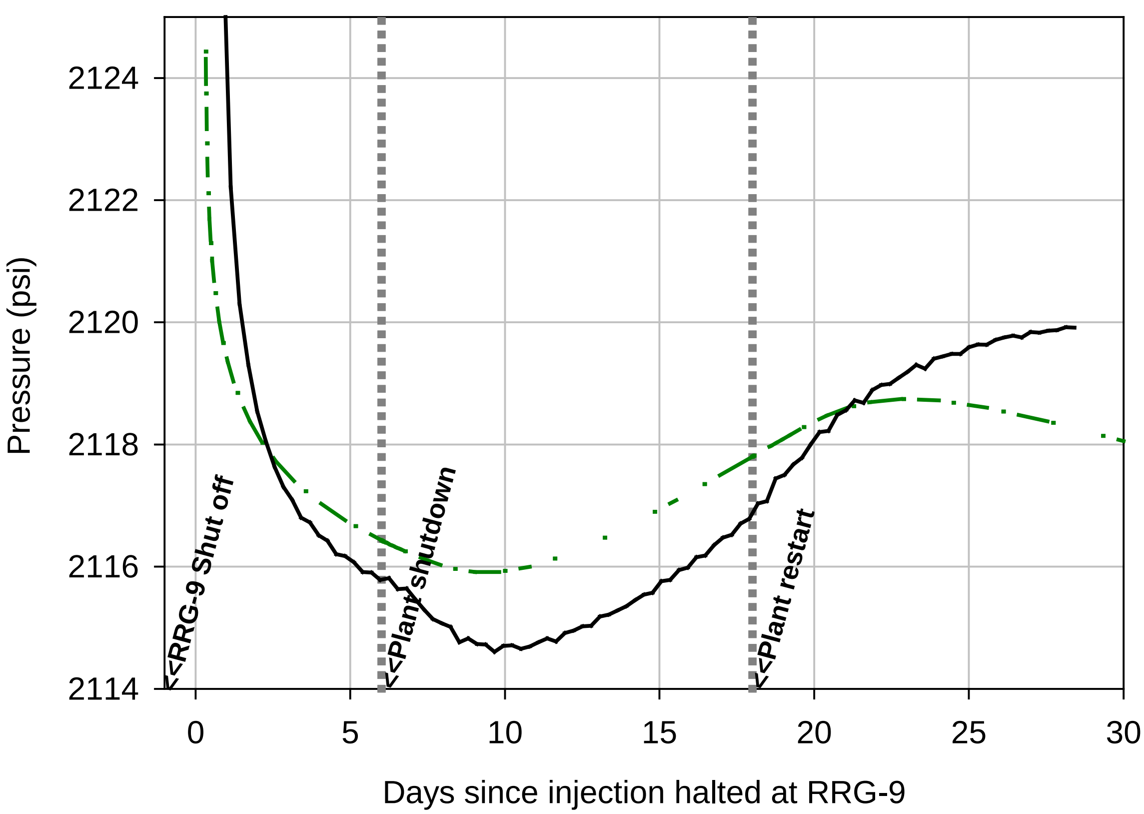

Figure 8. Observed, and simulated, pressure in well RRG-9 during plant shutdown in May 2015. RRG-9 was shut in on April 28 to examine its response to plant operation changes. Plant operations, and flow from and to other wells, stopped 6 days later and resumed 18 days later. Reinjection at RRG-9 resumed on May 27. Prior to shut-in, pressure was relatively steady at 2440 psi. Dashed vertical lines show plant shutdown period. Solid curve shows observed pressure response; dashed curve shows pressure response for a 2-well model with a single aquifer sandwiched between aquicludes.

3.3.2 Stepped-Rate Test Response

As described earlier, pressure response to increasing flow rates during the stepped-rate tests indicated some pressure-dependent permeability and/or compressibility. While the rapid transition to an apparent steady-state flow/pressure relationship makes the interpretation of the late time periods of the stepped-rate tests difficult, steps before that transition should provide some indication of the pressure dependence of transmissivity and storativity. Plots of response during that period suggest a strong pressure-dependent permeability in the first (February 2012) test, but not in the subsequent tests (Figure 9) that followed months of injection. This may reflect increases in permeability in the near-well region, associated with thermal contraction, that reduced the later response to changes in effective stress.

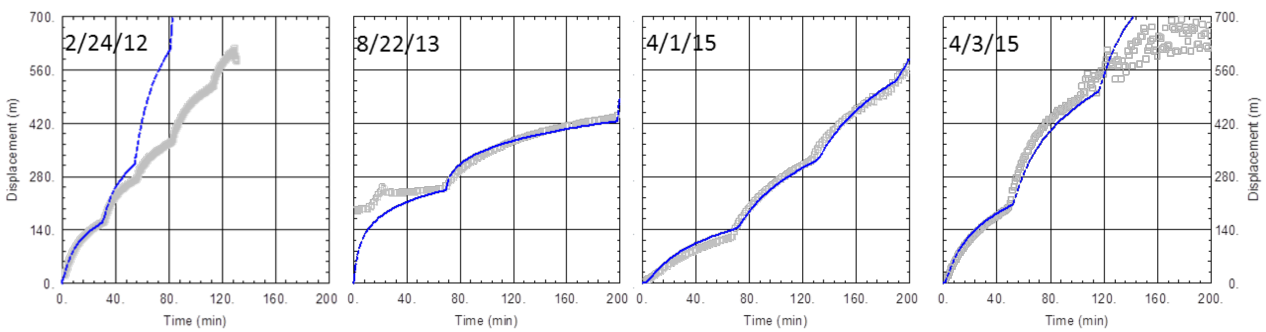

Figure 9. Plots of the first 200 minutes of each of four separate stepped-rate tests performed at RRG-9. Grey symbols are test data. Blue dashed curves are Theis-Hantush stepped-rate test curves fitted to each data set.

Rutqvist (1998) describes these stepped-rate tests in fractured rock as “hydraulic jacking tests,” because increasing pressure tends to expand near-wellbore fractures in successively larger amounts because of the nonlinear relationship between effective stress and fracture closure. That relationship is a result of the distribution of asperities on the fracture faces that provide increasing resistance to closure as more contacts are made. To examine the relative changes in permeability and/or storativity that might be needed to provide a better fit to RRG-9 response during the 2012 pre-injection stepped-rate test, we ran simulations using a 1-D, axisymmetric, finite element model with pressure-dependent permeability tuned to provide improved fit of simulated pressure response to observed pressure response. We modeled pressure dependence of permeability using the following function (Klinkenberg, 1941)

$$k(p_e) = k_0 exp(-bp_e{}^y), \qquad \text{(Eq. 7)}$$

where $k(p_e)$ is the permeability measured at effective displacement pressure, k_0 is the permeability at zero displacement pressure, and b and y are fitting parameters.

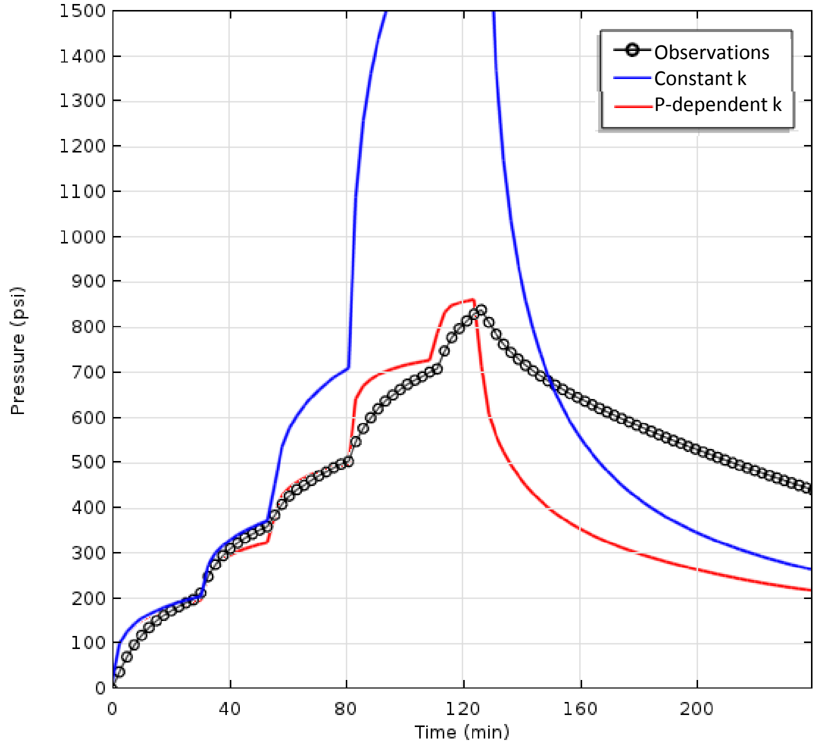

Figure 10. Comparison of observed pressure response (symbols) to the early part of a stepped-rate flow test to simulated response with a 1D radial flow model with constant permeability (blue curve) and with pressure-dependent permeability as described in the text (red curve).

Results demonstrate that inclusion of a nonlinear effective relationship between stress and permeability can produce a reasonable fit to observed pressure response, but the most striking result of such an analysis is that the pressure falloff, after a sequence of increasing flow rates, is inconsistent with increased local permeability. After injection stopped at 127 minutes, pressure remained relatively high, falling off much more slowly than predicted by the pressure-dependent permeability model. The response appears to reflect a condition under which permeability decreases faster than does the pressure.

4 CONCLUSIONS

The most striking feature of the response to cold-water injection at RRG-9 is the large overall increase in injectivity attained, and a general trend of accelerating improvement. In the ~2.5 years discussed here, an ~150-fold increase in injectivity has been achieved, an improvement greater than has been reported in any other thermal stimulation test. Because the larger part of the injectivity improvement has occurred over long timescales, it is likely related to the migration rate of the thermal front, and the attendant changes in permeability induced by associated rock contraction. We hypothesize that migration of the cooling front into zones of differing permeability could also produce the observed apparent acceleration trend, implying that the rate of improvement will decrease as the rate of migration of that front slows.

Additional information about the reservoir is largely obtained from relationships between pressure and flow measured during periodic stepped-rate injection tests performed as part of the project. Based on these tests and the long-term response, we conclude that a large fracture at approximately 5650 ft, identified in borehole televiewer logs and other data sources, increases the effective radius of RRG-9, so that storativity estimates based on hydraulic response give artificially high values. Assuming that storativity of the fractured quartzite is in the range of 2E-10 to 2E-8 Pa^{-1}, we infer that the effective radius of the anomalous aperture fracture is up to approximately one meter in radius. Based on estimates of the compressibility of fractured quartzite in the literature and the hydraulic response of well RRG-9, the initial background transmissivity of the reservoir was approximately 3E-14 m^3, and flow around the well is dominantly radial to a distance of approximately 2 to 20 meters. At that distance, the pressure buildup cone around the well intersects a condition that limits further pressure increase. While several mechanisms could explain that behavior, we suggest that at that distance, flow intersects an extensive region of high permeability.

Calculated hydraulic parameters appeared to increase with pressure during the first injection test, and the higher values were reproduced during the second stepped-rate test. Based on the latter data, the apparent transmissivity and storativity are on the order of 4E-5 m cm^2 and 1E-4 m Pa^{-1}. Based on type-curve analysis of the data, we conclude that the apparent pressure dependence of fitted hydraulic parameters reflects near-well fracture compliance that increased the effective radius of the wellbore during the first test.

The analysis and simulations here are intended to demonstrate how various features of the long-term hydraulic record can be interpreted, and what constraints they place on geologic interpretation, rather than as a best estimate of hydraulic conditions at the injection well.

5 REFERENCES

Allman, D.W., Tullis, J.A, Dolenc, M.R., Thurow, T.L. and Skiba P.A., 1982. Raft River Monitor Well Potentiometric Head Responses and Water Quality as Related to the Conceptual Ground-Water Flow System, EG&G Idaho Inc. Technical Report (EGG-2215), Vol. II, prepared for the US Department of Energy, Idaho Operations Office.

Aqui, A. and Zarrouk, S., 2011. Permeability enhancement of conventional geothermal wells, New Zealand Geothermal Workshop 2011 Proceedings, Auckland, New Zealand.

Ayling, B., Molling, P., Nye, R., and Moore, J., 2011. Fluid geochemistry at the Raft River geothermal field, Idaho: New data and hydrogeological implications, Proceedings, Thirty-Sixth Workshop on Geothermal Reservoir Engineering, Stanford University, Stanford, California, January 31–February 2, 2011.

Bradford, J., Ohren, M., Osborn, W., McLennan, J., Moore, J., and Podgorney, R., 2014. Thermal Stimulation and Injectivity Testing at Raft River, ID EGS Site, Proceedings, Thirty-Ninth Workshop on Geothermal Reservoir Engineering, Stanford University, Stanford, California, February 24–26, 2014.

Dolenc, M.R., Hull, L.C., Mizell, S.A., Russell, B.F., Skiba, P.A., Strawn, J.A., and Tullis J.A., 1981. Raft River Geoscience Case Study, EG&G Idaho Inc. Technical Report (EGG-2125), Vol. I, prepared for the US Department of Energy, Idaho Operations Office.

Duffield, G.M., 2007. AQTESOLV for Windows Version 4.5 User's Guide, HydroSOLVE, Inc., Reston, VA.

Earlougher Jr, R.C, 1977. Advances in Well Test Analysis, Dallas, TX.

Engelder, T. and Scholz, C., 1981. Fluid flow along very smooth joints at effective pressures up to 200 megapascals, Geophysical Monograph 24, 147–152.

Fekete Associates, Inc., 2014. Well Testing Fundamentals poster, http://fekete.com/consulting/well-testing-and-rate-transient-analysis/Pages/Default.aspx, Web. November, 2013.

Flores-Armenta, M. and Tovar-Aguado, R., 2008. Thermal fracturing of Well H-40, Los Humeros Geothermal Field, GRC Transactions 32, 445–448.

Grant, M.A., 2012. Thermal stimulation: the easiest and least recognised mechanism of permeability change. Paper presented at US/NZ geothermal workshop.

Grant, M.A., Clearwater, J., Quinao, J., Bixley, P.F., and Brun, M.L., 2013. Thermal stimulation of geothermal wells: A review of field data Proc., 38th Workshop on geothermal reservoir engineering, Stanford University.

Kitao, K., Ariki, K., Hatakeyama, K., and Wakita K., 1990. Well stimulation using cold-water injection experiments in the Sumikawa Geothermal Field, Akita Prefecture, Japan, Geothermal Resources Council Transactions 14.

Klinkenberg, L.J., 1941. Klinkenberg, L.J. 1941. The permeability of porous media to liquids and gases. Drill. & Prod. Prac. 200.

Kruseman, G.P.; de Ridder, N.A., 1990. Analysis and Evaluation of Pumping Test Data (Second Ed.). Wageningen, The Netherlands: International Institute for Land Reclamation and Improvement. ISBN 90-70754-20-7.

Marin, E., 2010. Characteristic dimensions for heat transfer, Lat. Am. J. Phys. Educ. 4, 56–60.

Plummer, M., 2013. Insights into Cold Water Injection Stimulation Effects through Analytical Solutions to Flow and Heat Transport, Transactions 37, Geothermal Resources Council.

Hantush, M.S., 1961a. Drawdown around a partially penetrating well, Jour. of the Hyd. Div., Proc. of the Am. Soc. of Civil Eng. 87, 83–98.

Hantush, M.S., 1961b. Aquifer tests on partially penetrating wells, Jour. of the Hyd. Div., Proc. of the Am. Soc. of Civil Eng. 87, 171–194.

Palmer C., Blowes, D., Frind, E., and Molson, J., 1992. Thermal energy storage in an unconfined aquifer – 1. Field Injection Experiment. Water Resources Research 28, 2845–2856.

Pasikki, R., Libert, F., Yoshioka, K., and Leonard R., 2010. Well stimulation techniques applied at the Salak Geothermal Field, Proceedings World Geothermal Congress 2010.

Rutqvist, J., Noorishad, J., Tsang, C., and Stephansson, O., 1998. Determination of fracture storativity in hard rocks using high-pressure injection testing, Water Resources Research 34, 2551–2560.

Thiem, G., 1906. Hydrologische Methoden; Gebhardt, Leipzig.

Theis, C.V., 1935. The relation between the lowering of the piezometric surface and the rate and duration of discharge of a well using groundwater storage, Am. Geophys. Union Trans. 16, 519–524.

Tulinius, H., Correia, H., and Sigurdsson, O., 2000. Stimulating a high enthalpy well by thermal cracking, Proceedings World Geothermal Congress 2000, Kyushu-Tohoku, Japan.

Williams, P.L., Pierce, K.L., McIntire, D.H., and Schmidt, P.W., 1974. Preliminary geologic map of the southern Raft River area, U.S.G.S. Open File Report, 1:24,000.